Journal of Power Sources 191 (2009) 528–533

Contents lists available at ScienceDirect

Journal of Power Sources

journal homepage: www.elsevier.com/locate/jpowsour

Microstructure and electrochemical characterization of solid oxide fuel cells fabricated by co-tape casting

Xiaoliang Zhou[a,b,c], Kening Sun[a,c,*], Jie Gao[c], Shiru Le[a,c], Naiqing Zhang[a,c], Peng Wang[b]

[a] Science Research Center, Research Academy of Science and Technology, Harbin Institute of Technology, Harbin 150001, PR China
[b] School of Municipal and Environmental Engineering, Harbin Institute of Technology, Harbin 150090, PR China
[c] Department of Applied Chemistry, Harbin Institute of Technology, No. 92 of West Dazhi Street, PO Box 211, Harbin 150001, PR China

ARTICLE INFO

Article history:
Received 29 December 2008
Received in revised form 1 February 2009
Accepted 2 February 2009
Available online 13 February 2009

Keywords:
SOFC
Yttria-stabilized zirconia (YSZ)
Tape casting
Thin films
EIS

ABSTRACT

A co-tape casting technique was applied to fabricate electrolyte/anode for solid oxide fuel cells. YSZ and NiO–YSZ powders are raw materials for electrolyte and anode, respectively. Through adjusting the Polyvinyl Butyral (PVB) amount in slurry, the co-sintering temperature for electrolyte/anode could be dropped. After being co-sintered at 1400 °C for 5 h, the half-cells with dense electrolytes and large three phase boundaries were obtained. The improved unit cell exhibited a maximum power density of 589 mW cm^{-2} at 800 °C. At the voltage of 0.7 V, the current densities of the cell reached 667 mA cm^{-2}. When the electrolyte and the anode were cast within one step and sintered together at 1250 °C for 5 h and the thickness of electrolyte was controlled exactly at 20 μm, the open-circuit voltage (OCV) of the cell could reach 1.11 V at 800 °C and the maximum power densities were 739, 950 and 1222 mW cm^{-2} at 750, 800 and 850 °C, respectively, with H_2 as the fuel under a flow rate of 50 sccm and the cathode exposed to the stationary air. Under the voltage of 0.7 V, the current densities of cell were 875, 1126 and 1501 mA cm^{-2}, respectively. These are attributed to the large anode three phase boundaries and uniform electrolyte obtained under the lower sintering temperature. The electrochemical characteristics of the cells were investigated and discussed.

1. Introduction

Solid oxide fuel cells (SOFCs) are promising candidates for many power generation schemes from small systems of a few watts up to megawatt-sized power plants and have been considered as the premium power generation devises in the 21st century as they have demonstrated high energy conversion efficiency, high power density, extremely low pollution, in addition to flexibility in using hydrocarbon fuel [1]. The conventional materials for SOFC are $La_{1-x}Sr_xMnO_3$ (LSM), NiO, and yttria-stabilized zironia (YSZ), respectively. The LSM–YSZ is used as composite cathode, and pure YSZ as electrolyte. The components of the electrolyte/anode half-cell include: (a) the electrolyte (8 mol% Y_2O_3–stabilized ZrO_2 (YSZ)); (b) the anode, a Ni/YSZ cermet [2]. The YSZ/YSZ-Ni materials are currently used by many researchers such as Versa Power System, Siemens Westinghouse Power Corporation, H.C. Starck, CeramTec and TOFC [3–7].

The commonly used methods for preparing the electrolyte/anode half-cells could be separated into two steps: (1) the preparation of anode substrate; (2) the coating of electrolyte on anode substrate [8–11]. Several methods for preparing SOFC components have been investigated, including sol–gel processing [12], electrochemical vapor deposition (EVD), screen printing [13], chemical vapor deposition (CVD) [14], tape casting [15–18], spray pyrolysis [19,20] and so on. Among all these methods, tape casting is regarded as a cost-effective and simple process for mass production. Therefore, we applied co-tape casting method for preparing the electrolyte/anode half-cell within one step in view of the advantages of co-tape casting as listed below:

(1) Best way to form large-area, thin, flat parts;
(2) Easy to be applied in the industrial production;
(3) Electrolyte and anode can be cast together within one step;
(4) The thickness of anode and electrolyte can be controlled exactly;
(5) The cost is very low.

During the fabrication of the electrolyte/anode half-cell, it is required to tape cast three layers: (a) the electrolyte; (b) the anode functional layer (AFL); (c) the anode substrate layer (ASL). They are cast one by one from electrolyte to anode substrate. The thick-

* Corresponding author at: Science Research Center, Research Academy of Science and Technology, Harbin Institute of Technology, Harbin 150001, PR China. Tel: +86 451 86412153; fax: +86 451 86412153.
E-mail address: keningsun@yahoo.com.cn (K. Sun).

0378-7753/$ – see front matter © 2009 Elsevier B.V. All rights reserved.
doi:10.1016/j.jpowsour.2009.02.008

ness of each layer can be controlled by means of controlling the height of blade during the tape casting operation [21]. After the process of drying, the multi-layer green tape is sintered together at high temperature. However, the anode needs a relatively low sintering temperature to prevent powders from agglomeration in order to obtain a large three phase boundaries (TPBs). TPBs are directly responsible for the performance of the cells. As for the electrolyte, a relatively high temperature is needed to obtain the dense electrolyte which can isolate fuels and air and transmit O^{2-} effectively [22]. Therefore, the samples are sintered at different temperatures for achieving proper processing conditions. First the suitable sintering temperature for anode was determined, and then the amount of PVB in the slurry to make electrolyte dense was adjusted. PVB, a high polymer with large molecular weight, is very crucial for tape casting to build the network in the anode; however, PVB will be burning at high temperature, simultaneously resulting in many pores. These pores pose a negative influence on the electrolyte, lowering the density and the ionic conductivity of electrolyte. Therefore, decreasing the amount of PVB is an effective way to reduce the pores of the electrolyte, finally resulting in the reducing of the sintering temperature. Electrochemical characteristics of the single cell were performed and discussed.

2. Experimental details

2.1. Cell fabrication

Commercial YSZ (Average particle size 40 nm, E-type, TOSOH, Japan), NiO (Average particle size 0.67 μm, Caiyu, China), and NiO (Average particle size 3–7 μm, SCRC, China) were used for cell fabrication. The electrolyte/anode half-cell contains three layers: electrolyte layer, anode functional layer (AFL), and anode substrate layer (ASL). The fabricating process for half-cell production is outlined in Fig. 1.

The electrolyte slurry was composed of TOSOH YSZ, solvent, and dispersant. The mixture of methyl ethyl ketone (MEK) (60 mL) and ethanol (150 mL) was used as a solvent. A certain amount of YSZ (100 g) and glycerol trioleate (GTO) (2.5 mL) was added as the ceramic powders and a dispersant. The slurry was ball-milled for 24 h, and then the plasticizer and binder were added into the slurry. A required ratio of polyethylene glycol (PEG) (4.6 g) and Diethyl-ophthalate (PHT) (4 mL) was used as the plasticizers, and a certain amount of PVB was used as binder (4–12 wt%). The slurry was then ball-milled for 24 h continuously. After de-gassed by vacuum, the slurry was cast on a plastic membrane by the "doctor blade" method and allowed to dry in air for several minutes.

The processes for AFL and ASL are the same with electrolyte. But material compositions for the different layers are different. The NiO powders used in AFL were purchased from Caiyu Chemical Company, and the ratio of NiO–YSZ mixture in AFL is 60:40. The NiO powders used in ASL were purchased from SCRC, China, and the ratio of NiO–YSZ in ASL is 65:35, besides, starch was added into the ASL as pore former (10–15 wt%). The solvent, dispersant, plasticizer of AFL and ASL layers are very similar with that of electrolyte.

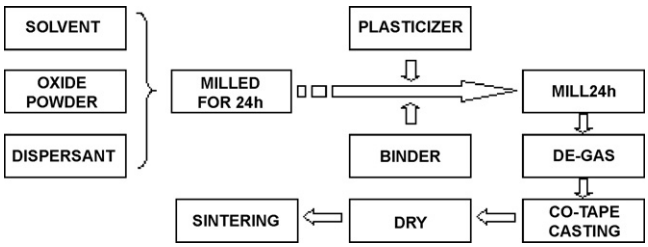

Fig. 1. Sketch of fabricating process for the electrolyte/anode half-cell.

The slurry of electrolyte was cast first. After several minutes, AFL slurry was cast on the top of electrolyte, and then ASL slurry was cast on the top of AFL. After drying overnight at room temperature, the multi-layer green tape was co-sintered at 1250 and 1400 °C in air for 5 h, respectively.

The composite cathode composing of LSM/YSZ was coated on the co-sintered electrolyte/anode half-cell by a screen printing process, and then sintered at 1200 °C for 2 h.

2.2. Electrochemistry testing

Silver wires were used as current collectors and adhered by silver paste on the cathode and the anode substrate. The cell was assembled in a zirconia tube with conductive adhesive silver paste and placed in a furnace [23]. Arbin fuel cell testing system (Germany) was employed to measure current–voltage curves of unit cells. The *I–V* and *I–P* tests were carried out at 800 °C using 50 sccm flow rate H_2 fuel with humidity of approximately 3%. NiO/YSZ composite ceramic was first reduced into Ni/YSZ cermet *in situ* under H_2 fuel environment at SOFC operating temperature of 800 °C. The tests characterize the open-circuit voltage (OCV) of the cell and ensure that there is little cross-leak or short circuit in the electrolyte and that there is a good seal between the components.

A PARSTAT 2273 advanced electrochemical system was employed for electrochemical impedance spectra (EIS) measurement. The EIS measurements were made over the frequency range of 10 Hz–100 kHz with the applied amplitude of 5 mV under open circuit. The measured spectra were fitted to the equivalent circuit by the nonlinear least square fitting software, ZSimpWin, developed by Bruno Yeum.

2.3. Microstructure characterization

After testing, some of the cells were fractured and cross-sections and surfaces of cells were examined under a Hitachi S-570 scanning electron microscope (SEM).

3. Results and discussion

3.1. Influence of organic additive PVB

3.1.1. Microstructures

PVB, a commonly used binder, should be adjusted to make the electrolyte dense. It supplies the network that holds the entire chemical system together for further processing [21]. And YSZ particles are embedded in the network. Pores will be produced after the evaporation of solvent. The porous network constructed by PVB prevents YSZ particles from agglomerating. However, PVB will be burning at high temperature and resulting in many pores. These pores have the negative influence on the electrolyte. The reduction of the PVB amount is a fundamental way to densify the electrolyte. Cross-sections of electrolytes with different amount of PVB in the slurry are shown in Fig. 2. The symbol '*m*' stands for the weight ratio of PVB. All of these samples are sintered at 1400 °C for 5 h. Sample A with the largest amount of PVB has the poorest density. When the amount of PVB drops to 0.08, the sample B becomes denser than A. Sample C with the least amount of PVB has the densest electrolyte. This shows that the PVB should be used as a minimal content. However, if the amount of PVB is less than 0.04, the network cannot form and the green tape is easily fractured. Therefore, the proper value of *m* is 0.04. Besides, the thickness of electrolyte can be controlled exactly at 25 μm as shown in Fig. 2B and C.

3.1.2. The cell performances

Fig. 3 shows the *I–V* and *I–P* characteristics of SOFC unit cells with different amount of PVB at 800 °C. The maximum power den-

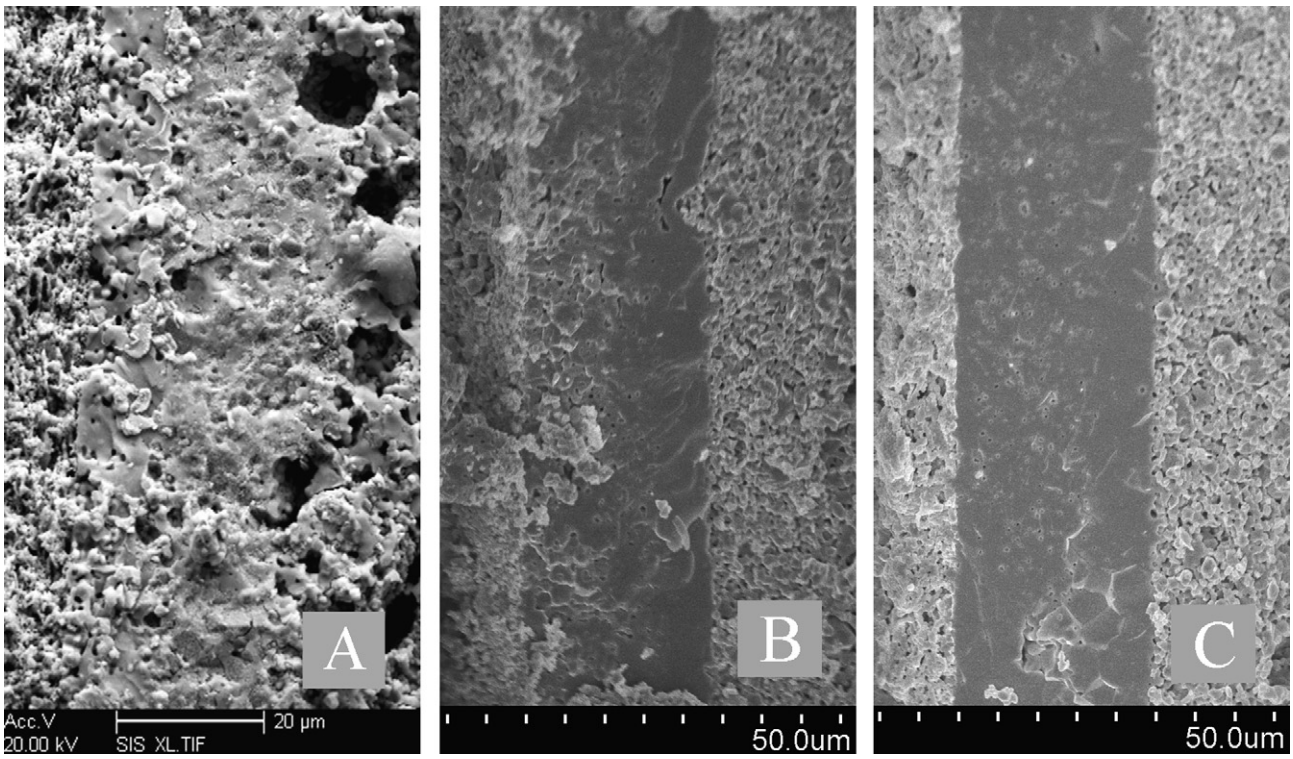

Fig. 2. SEM micrographs of cross-sections of electrolyte with different amount of PVB sintered at 1400 °C for 5 h. (A) $m = 0.12$; (B) $m = 0.08$; (C) $m = 0.04$.

sities of cell A–C are 340, 570, 589 mW cm^{-2}, respectively. At the voltage of 0.7 V, the current densities of the cell A–C are 328, 667 and 639 mA cm^{-2}, respectively. The open-circuit voltage (OCV) of cell A is 0.87 V which is much lower than the theoretical value of 1.19 V. This is caused by gas leakage through pores in electrolyte. In contrast, the OCVs of both B and C, higher than that of cell A, are about 1.0 V. This is attributed to the denser electrolytes of B and C. Though the densities of the electrolyte of B and C are different, they are gas tight as shown in Fig. 2B and C. Thus the OCVs are of the same value. The different densities between B and C lead to different ion-conductivities, and this will further lead to the different maximum power densities at higher current densities. However, the resistance of the load device prevented further evaluation of B and C at higher current densities. From the *I–P* curves, it is clear that the maximum power densities of B and C are expected to be higher than the measured values.

3.1.3. The electrochemical impedance performance

The electrochemical behaviors of unit cells were investigated by EIS measurement under open-circuit conditions. Fig. 4 shows Nyquist plots and its equivalent circuit of unit cells (A–C) under open-circuit and fuel cell operating conditions. The symbols were denoted as follows: R_s is the ohmic resistance of electrolyte and lead wires, CPE (Q) the constant phase element, R_1 the electrode resistance, and L is the inductance of lead wires. The process associated with the arc appears to be related to a charge transfer reaction at the electrode/electrolyte interface [24]. R_p is the polarization resistance [25]. The values of R_s and R_p were calculated by ZSimpWin program.

Table 1 shows the R_s and R_p values of cells A–C, and other researchers' results for comparison. It is clear that the R_s of A is bigger than that of B and C. This can be explained by the poor

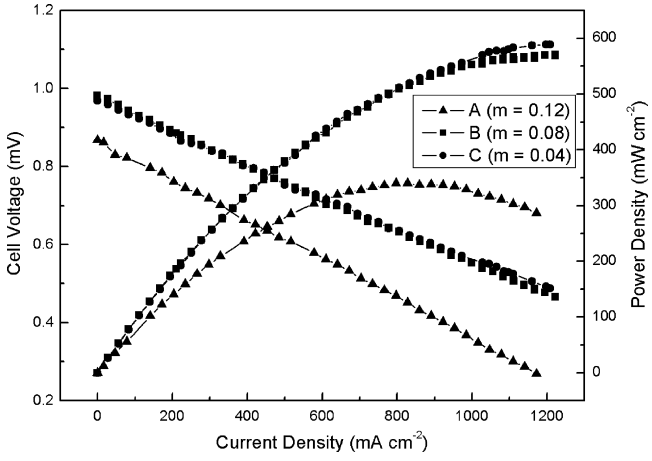

Fig. 3. *I–V* and *I–P* characteristics of SOFC unit cells sintered at 1400 °C for 5 h with different amount of PVB.

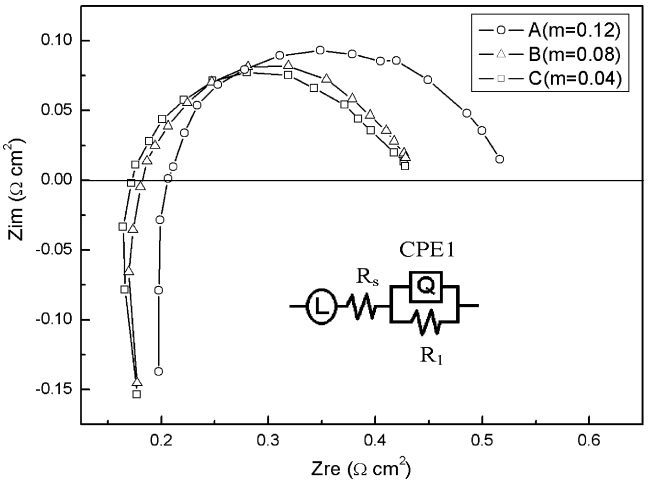

Fig. 4. Nyquist plots and equivalent circuit of unit cells under open circuit recorded at 800 °C.

Table 1
Electrochemical characteristics R_s and R_p of the cells at 800 °C and comparison with other researchers' results.

Symbol	R_s (Ω cm^2)	R_p (Ω cm^2)
A (m = 0.12)	0.185	0.350
B (m = 0.08)	0.168	0.269
C (m = 0.04)	0.161	0.251
J. Kong [26]	0.225	0.273
L. Besra [27]	0.3	0.7

electrolyte density of A, which leads to high electrical resistance. Compared with other results, the R_s and R_p values of cells B and C are smaller, indicating that fabricating the cells by co-tape casting and adjusting the content of PVB could improve the performance of anode and electrolyte.

3.1.4. Microstructure after electrochemical test

The SEM micrographs of the cross-section of a fractured unit cell after testing were surveyed, which were shown in Fig. 5. This unit cell had been tested for more than 20 h, and experienced three thermo-cycles. Cathode, electrolyte, AFL, ASL can be seen clearly in Fig. 5a. A small area in Fig. 5a is magnified as shown in (b). It can be seen in Fig. 5b that YSZ electrolyte is dense and connects well with AFL. The anode functional layer has small grain sizes, sufficient porosity as well as even distribution of the nickel phase, the YSZ ceramic phase and the pores. The interface between AFL and anode substrate can be observed clearly. The microstructure of anode substrate is coarser and more porous than that of AFL benefiting the fuel gas and vapor transmission in it. The microstructure of this tested unit cell is still in good condition.

3.2. Cell performance co-sintered at a lower temperature

3.2.1. Microstructures

In this section, the electrolytes were sintered at a lower temperature of 1250 °C for 5 h. Microstructures are shown in Fig. 6. As shown in (a) and (b), there are many pores in electrolyte. But most pores are pin-holes and closed. It could be seen that the thin YSZ electrolyte films were uniformly continuous, dense, adhered well to the porous anode substrate. The OCV is above 1.11 V at 800 °C as shown in Fig. 8, which was close to the theoretical one of 1.19 V, indicating the film was dense enough and little gas leakage existed. Electrolyte with a thickness of 20 μm has a uniform structure. In anode functional layer (AFL), both Ni and YSZ particles sizes are less than 2 μm. Pores, Ni, and YSZ distribute uniformly. Thus, there is a large three phase boundaries in AFL. The thickness of AFL is also controlled at 20 μm. From AFL to ASL, the porosity changed a lot. Starch was added in ASL as pore former. The pore sizes produced by starch are form 10 to 20 μm. The large porosity in ASL enables the fast fuel supply and quick exhaust removal. In order to evaluate the leakage of the half-cells, the leak test was carried out and the results indicated that for the samples sintered at 1400 and 1250 °C, there occurred almost no leakage of the half-cells. This showed that sintering at relatively low temperature 1250 °C can satisfy the requirement for application of SOFC.

Fig. 7 shows SEM micrographs of surface of anode after sintered at 1250 °C for 5 h. In Fig. 7a, pores are distributed uniformly, and the average pore sizes are about 5 μm. As shown in Fig. 7b, the YSZ particle size is less than 1 μm and Ni particle size is over 2 μm. Small YSZ particles surround large Ni particle to prevent Ni from agglomeration. YSZ particles and Ni particles connected with each other very well. They formed a strong network to afford enough mechanical strength and gas channels.

3.2.2. The cell performances

Cells were sintered at 1250 °C for 5 h with OCVs above 1.11 V at 800 °C as shown in Fig. 8. The OCV of the samples sintered at 1250 °C is different with that the samples sintered at 1400 °C. Probably this is due to the fact that the difference may come from the instrumental error such as the inaccuracy of temperature control of single cells test equipment or the water bubbler for fuel gas. The power densities of the cell were 739, 950 and 1222 mW cm^{-2} at 750, 800 and 850 °C, respectively, with H_2 at a flow rate of 50 mL min^{-1} as fuel and ambient air as oxidant. On the other side, at the temperatures of 750, 800 and 850 °C and under the voltage of 0.7 V, the current densities of cell were 875, 1126 and 1501 mA cm^{-2}, respectively. These results are higher than that sintered at 1400 °C for 5 h. This is attributed to the large anode three phase boundaries and uniform electrolyte which could be obtained under the lower sintering temperature of 1250 °C for 5 h.

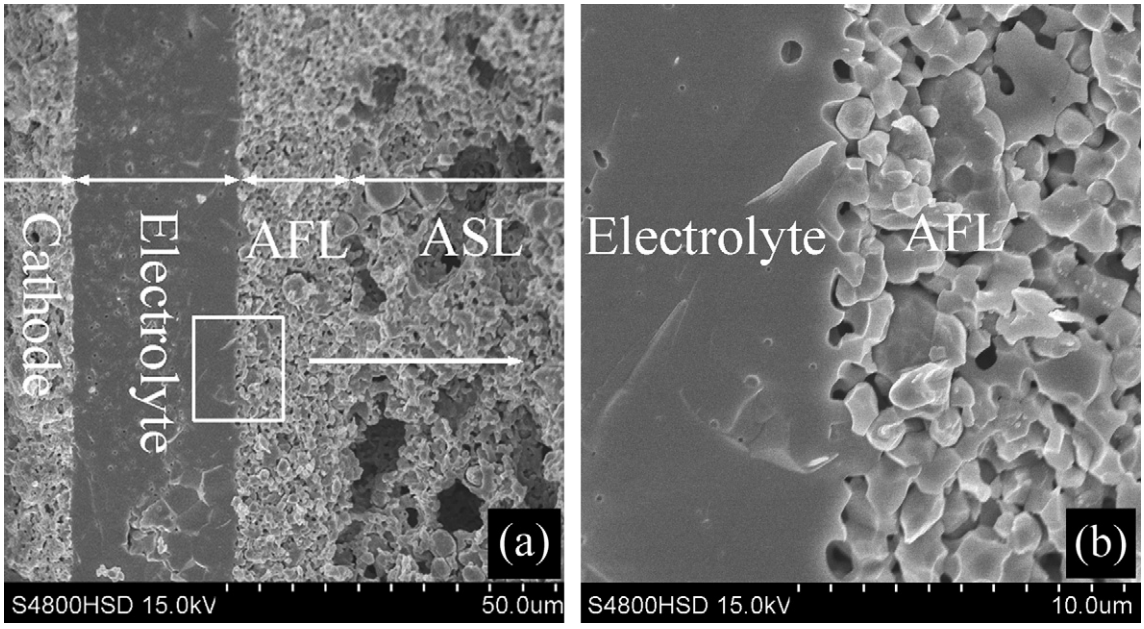

Fig. 5. SEM micrographs of cross-sections of unit cells after electrochemistry testing.

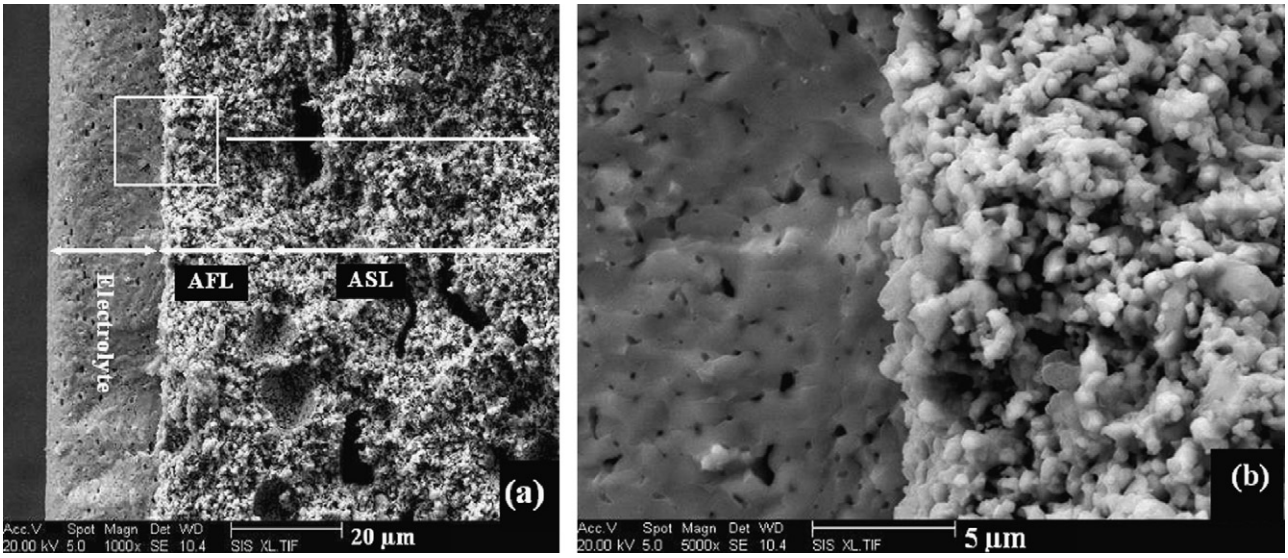

Fig. 6. SEM micrographs of cross-sections of electrolyte/anode after sintered at 1250 °C for 5 h.

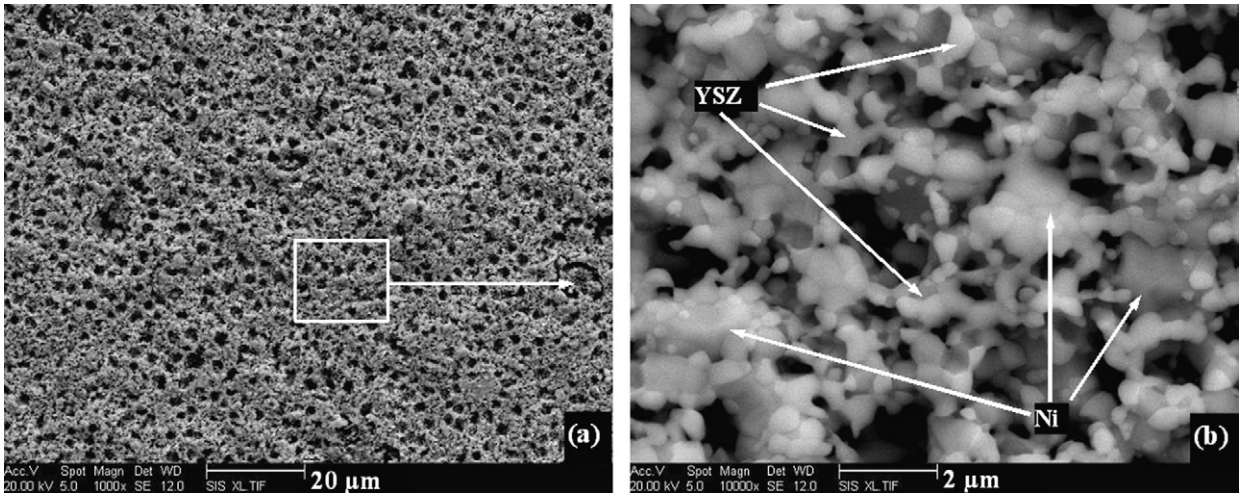

Fig. 7. SEM micrographs of surface of anode after sintered at 1250 °C for 5 h.

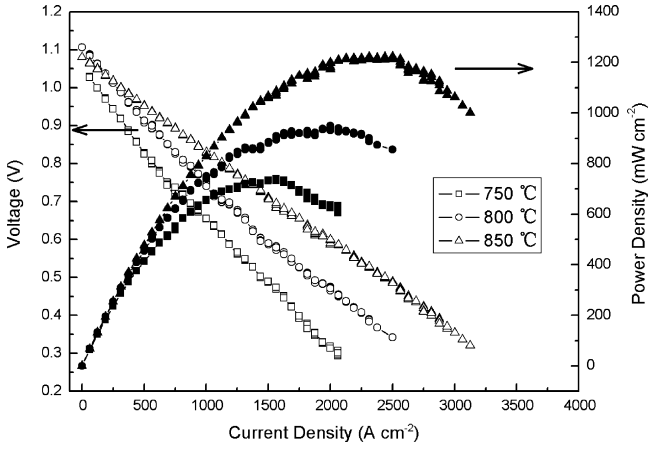

Fig. 8. The electrochemical performance of the single cell recorded at different temperatures.

3.2.3. *The electrochemical impedance performance*

The electrochemical behaviors of the cell were investigated by EIS measurement under open-circuit conditions. Fig. 9 showed EIS response and its equivalent circuit of the cell under open-circuit and fuel cell operating conditions. The solid line in Fig. 9 is the fitted result of the ZSimpWin program. The impedance diagram is composed of two semicircles referred to as HF (for high frequency) and MF (for middle frequency). The observation of two clearly separated arcs in the frequency domain indicates that H_2 oxidation at Ni-YSZ cermet electrodes is controlled by at least two electrode processes at the Ni surface (the first electrode process). The process associated with the high frequency arc appears to be related to a charge transfer reaction at the electrode/electrolyte interface (the second electrode process) [13].

The polarization resistance R_p is defined as [14]: $R_p = R_1 + R_2$. R_1 and R_2 are the electrode resistances. The values of the symbols were illustrated in Table 2. R_2 is smaller than R_1, which reveals that the effect of charge–transfer reaction appears to be more dominant. In other words, surface dissociation/diffusion step is easier than charge–transfer reaction. This means the microstructure of the anode, especially anode functional layer, was fabricated fine and the

Table 2
Electrochemical characteristics of the cell at different temperatures and comparison with other researchers' results.

Temperature	L (H cm^2)	R_s (Ω cm^2)	Q_1 (F cm^{-2})	n	R_1 (Ω cm^2)	Q_2 (Ω^{-1} cm^{-2} s^{-n})	n	R_2 (Ω cm^2)	R_p (Ω cm^2)
750 °C	1.361E-7	0.154	0.196	0.732	0.231	0.01204	0.645	0.178	0.409
800 °C	1.641E-7	0.113	0.218	0.711	0.191	0.01818	0.571	0.081	0.272
850 °C	1.387E-7	0.109	0.336	0.634	0.091	0.00198	0.880	0.027	0.118
Other researchers' results at 800 °C:									
J. Kong [26]		0.225			0.209			0.064	0.273
L. Besra [27]		0.3							0.7

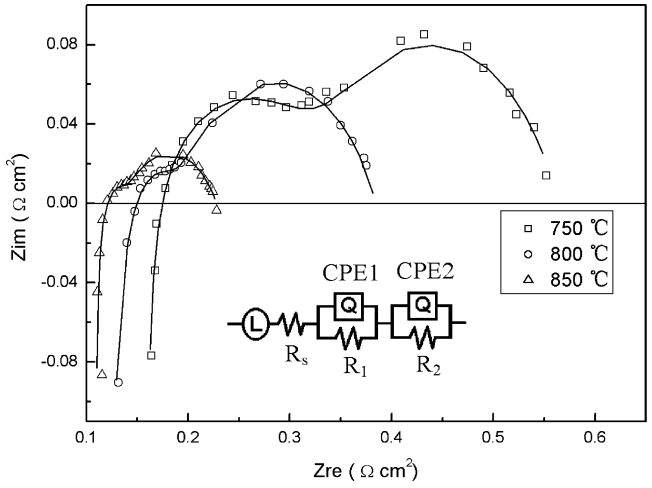

Fig. 9. Nyquist plots and equivalent circuits of the cell under open circuit at 750, 800 and 850 °C, respectively.

distribution of the two phases was homogeneous, thus the interfacial resistance reduced and then the cell performance could be increased. Both R_s and R_p are lower than some researchers' results as well. This means the cell has low ohmic resistance and polarization resistance. However, R_p is larger than R_s. Polarization resistance appears to be more dominant. R_p is concerned with the electrical resistance of the electrodes including the anode and the cathode. Therefore, through optimizing the electrode microstructure, we can decrease the values of R_p, further improving the cell performance.

4. Conclusion

In the present study, co-tape casting was applied to fabricate electrolyte/anode half-cell. The preparation steps were simplified and the co-sintering temperature was as lower as 1250 °C. The thickness of electrolyte was controlled exactly at 20 μm, and electrolyte was dense enough to ensure the OCV above 1.11 V which was close to the theoretical one of 1.19 V. The anode functional layer had a uniform structure and large three phase boundaries. In anode substrate layer, small YSZ particles surrounded the large Ni particles, and they formed a strong network to afford enough mechanical strength and gas channels. Under the voltage of 0.7 V, the current densities of cell at 750, 800 and 850 °C were 875, 1126 and 1501 mA cm^{-2}, respectively. Maximum power densities could reach 739, 950 and 1222 mW cm^{-2} at 750, 800 and 850 °C, respectively, with H_2 as the fuel under a flow rate of 50 sccm and the cathode exposed to the stationary air. Both the ohmic resistance and polarization resistance are lower than some researchers' results, and the polarization resistance is dominant which needs to be improved in further works.

Acknowledgement

This project is financially supported by Development Program for Outstanding Young Teachers in Harbin Institute of Technology (No.HITQNJS.2008.056), China Postdoctoral Science Foundation (No.20070420865), and Natural Science Foundation of China (No.90510006).

References

[1] S.C. Singhal, K. Kendal (Eds.), High Temperature Solid Oxide Fuel Cells: Fundamental, Design and Applications, Elsevier, 2003, pp. 15–55.
[2] D. Simwonis, H. Thulen, F. Dias, et al., J. Mater. Process. Technol. 92–93 (1999) 107–111.
[3] F. Tietz, H. Buchkremer, D. Stover, Solid State Ionics 152–153 (2002) 373–381.
[4] D. Gosh, G. Wang, R. Brule, et al., The Electrochemical Society, Pennington, NJ, 1999, p822.
[5] M. Pastula, R. Boersma, D. Prediger, et al., The European Fuel Cell Forum, Oberrohrdorf, Switzerland, 2000, 123.
[6] D. Waldbillig, A. Wood, D.G. Ivey, J. Power Sources 145 (2005) 206–215.
[7] M. Willams, J. Strakey, S. Singhal, J. Power Sources 131 (2004) 79–85.
[8] S. Souza, S. Visco, L. Jonghe, Solid State Ionics 98 (1997) 57–61.
[9] Y. Leng, S. Chan, K. Khor, et al., Int. J. Hydrogen Energy 29 (2004) 1025–1033.
[10] F. Zhao, A.V. Virkar, J. Power Sources 141 (2005) 79–95.
[11] S.D. Kim, H. Moon, S.H. Hyun, et al., J. Power Sources 163 (2006) 392–397.
[12] A. Sanson, P. Pinasco, E. Roncari, J. Eur. Ceram. Soc. 28 (2008) 1221.
[13] P. Timakul, S. Jinawath, P. Aungkavattana, Ceram. Int. 34 (2008) 867.
[14] S. Preusser, U. Stimming, K. Wippermann, Electrochim. Acta 39 (1994) 1273.
[15] C. Suciu, A.C. Hoffmann, A. Vik, F. Goga, J. Chem. Eng. 138 (2008) 608.
[16] G.J. Wright, J.A. Yeomans, J. Power Sources 159 (2006) 1048.
[17] P. Timakul, S. Jinawath, P. Aungkavattana, Mater. Sci. Eng.: A 420 (2006) 171.
[18] P. Albano Maria, A. Genova Luis, B. Garrido Liliana, Plucknett Kevin, Ceram. Int. 34 (2008) 1983.
[19] M.F. García-Sánchez, J. Peña, A. Ortiz, G. Santana, J. Fandiño, M. Bizarro, F. Cruz-Gandarilla, J.C. Alonso, Solid State Ionics 179 (2008) 243–249.
[20] M.F. García-Sánchez, J. Peña, A. Ortiz, G. Santana, J. Fandiño, M. Bizarro, F. Cruz-Gandarilla, J.C. Alonso, J. Eur. Ceram. Soc. 28 (2008) 779.
[21] R.E. Mistler, E.R. Twiname, Tape Casting Theory and Practice, The American Ceramic Society, Westerville, Ohio, 2000, p.83.
[22] M. Han, S. Peng, Solid Oxide Fuel Cell Components and Manufacture Processes, Chinese Science Press, Beijing, 2004, p. 2 (in Chinese).
[23] J.S. Qiao, K.N. Sun, N.Q. Zhang, et al., J. Power Sources 169 (2007) 253–258.
[24] S.P. Jiang, S.P.S. Badwal, Solid State Ionics 123 (1999) 209–224.
[25] M. Guillodo, P. Vernoux, J. Fouletier, Solid State Ionics 127 (2000) 99–107.
[26] J. Kong, K. Sun, D. Zhou, et al., J. Power Sources 166 (2007) 337–342.
[27] L. Besra, S. Zha, M. Liu, J. Power Sources 160 (2006) 207–214.